**MIRO1 controls energy production and proliferation of vascular smooth muscle cells**

Lan Qian, MBBS [1], Olha M. Koval, PhD [1], Benney T. Endoni, PhD [1,2], Denise Juhr, BS [1], Colleen S. Stein, PhD [1], Chantal Allamargot, PhD [3], Li-Hsien Lin, PhD [1], Deng-Fu Guo, PhD [4], Kamal Rahmouni, PhD [1,2,4,6], Ryan L. Boudreau PhD [1], Jennifer Streeter, MD, PhD [1], William H. Thiel, PhD[1], Isabella M. Grumbach MD, PhD [1,5,6]*

Short title: MIRO1 in smooth muscle proliferation

**Affiliations:**
[1] Abboud Cardiovascular Research Center, Division of Cardiovascular Medicine, Department of Internal Medicine, Carver College of Medicine, University of Iowa, Iowa City IA 52242, USA.

[2] Interdisciplinary Program in Molecular Medicine, University of Iowa,

[3] Central Microscopy Research Facility, University of Iowa,

[4] Department of Neuroscience and Pharmacology, University of Iowa,

[5] Free Radical and Radiation Biology Program, Department of Radiation Oncology, Holden Comprehensive Cancer Center, University of Iowa, Iowa City IA 52242, USA.

[6] Veterans Affairs Healthcare System, Iowa City, IA 52246, USA.

*To whom correspondence should be addressed:
Isabella Grumbach, MD, PhD
University of Iowa
Dept. of Internal Medicine
169 Newton Road
Iowa City, IA 52246
isabella-grumbach@uiowa.edu

The authors have declared that no conflict of interest exists.

## ABSTRACT

**Background:** The outer mitochondrial Rho GTPase 1, MIRO1, mediates mitochondrial motility within cells, but implications for vascular smooth muscle cell (VSMC) physiology and its roles in vascular diseases, such as neointima formation following vascular injury are widely unknown.

**Methods:** Carotid ligation was performed in an in vivo model of selective Miro1 deletion in smooth muscle cells. VSMC proliferation during the cell cycle and molecular mechanisms of smooth muscle cell proliferation were explored in cultured aortic VSMCs by imaging mitochondrial positioning and cristae structure and assessing the effects on ATP production, metabolic function and interactions with components of the electron transport chain (ETC). MIRO1 expression was analyzed in human coronary arteries, and its function was assessed via knockdown in human coronary artery VSMCs.

**Results:** Results revealed strong MIRO1 expression in VSMCs within human atherosclerotic plaques. MIRO1 facilitated VSMC proliferation and neointima formation by regulating mitochondrial positioning and PDGF-stimulated ATP production and respiration, critical for cell-cycle progression at G1/S. Deletion of Miro1 disrupted mitochondrial cristae structure, diminished ETC complex I activity, and impaired super complex formation. Notably, restoring MIRO1 function with a mutant lacking EF hands, which are essential for mitochondrial mobility, only partially rescued these effects. MIRO1 knockdown in human coronary artery VSMCs confirmed its pivotal role in mitochondrial function and VSMC proliferation.

**Conclusions**: This study highlights two key mechanisms by which MIRO1 regulates VSMC proliferation. First, it maintains ATP synthesis by preserving mitochondrial cristae integrity. Second, its $Ca^{2+}$-dependent EF hands enable ATP-dependent mitochondrial positioning. By linking mitochondrial motility and energy production to VSMC physiology, these findings position MIRO1 as a critical regulator of vascular remodeling and a potential target for therapeutic interventions.

**Keywords**: Mitochondria, MIRO1, proliferation, electron transport chain, smooth muscle, neointima

## INTRODUCTION

Mitochondria play a crucial role in various cellular functions throughout the cardiovascular system[1,2], yet their specific roles in vascular smooth muscle cells (VSMCs) of systemic arteries remain underexplored, particularly with respect to vasoproliferative diseases such as neointimal hyperplasia. Insights into these processes have largely stemmed from extending findings on cytosolic pathways. For instance, neointima formation has been shown to be inhibited either by promoting apoptosis via mitochondrial pathways [3-5] or by reducing mitochondrial ROS production through overexpression of uncoupling protein 2 or superoxide dismutase 2 [6-8].

Mitochondria dynamically adapt to cellular changes through fission and fusion, which modulate VSMC proliferation, migration, and neointima formation [9-11]. Moreover, over a decade ago Chalmers et al. showed that interfering with mitochondrial movement blocks VSMC proliferation [12]. Despite this, the molecular regulators governing mitochondrial mobility in VSMCs have remained largely understudied.

The outer mitochondrial membrane GTPase MIRO1 is essential for orchestrating mitochondrial positioning in many cell types, including neurons, lymphocytes, and various cancer cell lines [13-16]. MIRO1 contains two canonical EF-hand domains that are flanked by two GTPase domains and a C-terminal transmembrane domain that anchors MIRO1 to the outer mitochondrial membrane [17]. MIRO1 associates with trafficking kinesin-binding proteins (TRAKs), linking mitochondria to microtubules and myosin XIX [13-15,18]. These interactions are regulated by changes in intracellular $Ca^{2+}$ levels: when MIRO1 is not bound by $Ca^{2+}$/calmodulin, it links mitochondria to microtubules; when the EF hands are bound by $Ca^{2+}$, a conformational change causes mitochondria to dissociate from microtubules, arresting their movement [13]. In addition to playing a role in promoting mitochondrial mobility, MIRO1 is believed to control mitophagy through phosphorylation by the Pink/Parkin complex [19,20], and to facilitate the formation of

mitochondrial cristae via associations with the mitochondrial contact site (MICOS) complex and the mitochondrial intermembrane space bridging (MIB) complex [21].

Reports of MIRO1's diverse roles have prompted some investigations into its role in human diseases. For example, Miro1 mutations identified in humans (for example p.R272Q) have been linked genetically and pathophysiologically to Parkinson's disease [19,20,22].
Nevertheless, few studies have investigated its impact on cardiovascular disease. Cardiomyocytes isolated from neonatal rats lacking Miro1 were protected against phenylephrine-induced cardiomyocyte hypertrophy and mitochondrial fission [23]. However, its specific contributions to vascular pathologies remain unclear, with data from our laboratory highlighting MIRO1's impact on VSMC migration [24]. Emerging evidence positions MIRO1 as a regulator of cell proliferation of fibroblasts and [16,25,26]. Our group recently reported that cyclic changes in formation of mitochondrial ER contact sides (MERCS) that enable the transfer of $Ca^{2+}$ and other metabolites to mitochondria are required for cell proliferation and controlled by MIRO1 [25].

The goal of this study was to determine whether MIRO1 controls VSMC proliferation and, if so, to uncover the underlying mechanisms involved. We investigated the effects of MIRO1 manipulation on VSMC proliferation and the potential mechanism by which MIRO1 affects cell cycle progression, mitochondrial mobility, ATP production, and respiration. Additionally, we used a transgenic mouse model in which Miro1 was deleted specifically in VSMCs to test its effects on neointima formation in vivo.

## METHODS

### Data Availability

In accordance with the Transparency and Openness Promotion Guidelines, the authors declare that all supporting data and Supplemental Material are available from the corresponding authors upon reasonable request. The Supplemental Methods and the Major Resource Table can be found in the Supplemental Material.

### Animals

Animal studies were conducted in accordance with the NIH *Guide for the Care and Use of Laboratory Animals*, following protocols that were approved by the Institutional Animal Care and Use Committee (IACUC) of the University of Iowa. SMMHC-CreER□$^2$ mice, in which expression of tamoxifen-inducible Cre recombinase is driven by the smooth muscle myosin heavy chain (SMMHC) promoter, were obtained from Jackson Laboratory (Strain #019079). The Mitochondrial Rho1 GTPase LoxP (Floxed Miro1 conditional KO) mice were graciously provided by Dr. Janet Shaw (University of Utah) and backcrossed with C57BL/6J mice (Jackson Laboratories, Strain #000664). The VSMC-selective floxed Miro1 conditional knockout mice (SM-Miro1$^{-/-}$ mice) were generated by crossbreeding with SMMHC-CreER□$^2$ mice. Cre recombination was induced by intraperitoneal injection of tamoxifen (80 mg/Kg) for 5 days, followed by a 14-day break. SMMHC-CreER□$^2$ mice were injected with same dose of tamoxifen and used as a control for in vivo experiments. In vivo experiments were performed in male mice because the tamoxifen-inducible Cre recombinase in this model, whose expression is driven by the SMMHC promoter, is present on the Y-chromosome.

### Ligation of the common carotid artery and preparation of vessels for quantification of neointima and media

10–12-week-old SM-Miro1$^{-/-}$ mice and controls were fed high-fat chow for 3 weeks (D12492, 60 kcal% fat, Research Diets) and then, the animals were anesthetized, and survival surgeries of left common carotid artery ligation were performed [27]. A high fat diet was used to approximate human-like cholesterol levels and model metabolic conditions. This diet elevates serum cholesterol to approximately 250 mg/dL and slightly increases nonfasting glucose levels (~200 mg/dL), creating a metabolic profile close to that observed in humans with coronary artery disease (see https://www.jax.org/jax-mice-and-services/strain-data-sheet-pages/phenotype-information-380050). At 21 days after the surgery, the animals were anesthetized and underwent transcardiac perfusion with 10 ml of PBS, followed by fixation with 10 ml of 4% paraformaldehyde (PFA), at physiological pressure. The left (ligated) and right (non-ligated) common carotid arteries were excised at the carotid bifurcation and embedded for sectioning followed by Verhoeff Van Gieson (VVG) staining.

**Culture of vascular smooth muscle cells (VSMCs)**

Primary mouse aortic VSMCs were isolated enzymatically; incubation in elastase (1U/ml for 10 min at 37º) was performed to remove the adventitia. The medial layer of the aorta, which contains the VSMCs, was minced and incubated in 2 mg/ml collagenase type II digestion solution (Worthington Biochemical Corporation) for 2 hr. In early experiments, VSMCs were isolated from SM-Miro1$^{-/-}$ and littermate mice (referred to as SM-Miro1$^{-/-}$ VSMCs). In later experiments, VSMCs were isolated from Miro1$^{fl/fl}$ mice and had been transduced with adenovirus expressing Cre recombinase at a multiplicity of infection (MOI) of 50 for 2 weeks (referred to as MIRO1$^{-/-}$ VSMCs). VSMCs from littermate controls were subjected to the same procedure with empty vector control adenovirus.

**Statistical Analysis**

Statistical analysis was performed under guidance from the University of Iowa Department of Biostatistics. Data were analyzed using the GraphPad Prism 10.0 software and expressed as mean ± SEM. Normality and equal variance were assessed. Statistical comparisons between two groups were carried out using the unpaired t test when a normal distribution could be assumed. Otherwise, the Mann-Whiney U test was used. One-way analysis of variance (ANOVA) followed by Tukey's multiple comparisons was used for multiple group comparisons when a normal distribution could be assumed. Otherwise, the Kruskall-Wallis test with Dunn's multiple comparisons was used. Two-way ANOVA followed by Šidák multiple comparisons was used for grouped data sets. A *P*-value of <0.05 was considered significant, and p-values are indicated in the figures.

## RESULTS

### Loss of MIRO1 blocks neointima formation.

To study the effects of MIRO1 on smooth muscle cell biology after vascular injury, we generated a transgenic model in which MIRO1 is selectively deleted in smooth muscle cells after administration of tamoxifen (SM-MIRO1$^{-/-}$). Reduced levels of MIRO1 mRNA and protein in carotid arteries and the aorta were confirmed by immunohistochemistry, western blotting, and quantitative real time PCR (**Figure 1A**, **Figure S1A, B**). Mice of both the wild type and SM-MIRO1$^{-/-}$ genotypes were fed a high-fat diet for three weeks, and then vascular injury was induced by ligation of the common carotid artery. Three weeks after ligation, the mice were euthanized and neointima size was assessed. Neointima formation was robust in wild type mice and significantly reduced in SM-MIRO1$^{-/-}$ mice (**Figure 1B**). The neointimal and medial areas were smaller in the arteries from the SM-MIRO1$^{-/-}$ mice than in those of their wild type counterparts. Moreover, the neointimal area was decreased at 250 μm from the ligation site and the cumulative neointimal area over the first one mm of the carotid artery proximal to the ligation (**Figure 1C-F**). Immunohistochemical analysis in mouse carotid arteries after ligation revealed robust expression of MIRO1 in VSMCs of the neointima (**Figure 1G**). Lastly, we confirmed that MIRO1 is present in human coronary arteries. In a subject without a medical history of coronary disease, MIRO1 was present in the media. In human subjects with atherosclerotic disease, MIRO1 was expressed in both the media and the neointima, in cells also positive for smooth-muscle actin (**Figure 1H, Figure S2**). Moreover, in the atherosclerotic plaque, we detected the colocalization of MIRO1 with the proliferation marker Ki67. In some cells, both colocalized with smooth-muscle actin (**Figure S3**).

### Loss of MIRO1 reduces the proliferation of smooth muscle cells.

To determine the relevance of MIRO1 to cell proliferation, VSMCs were explanted from the aortas of SM-MIRO1$^{-/-}$ mice and cultured. Platelet-derived growth factor (PDGF) was used to

enhance cell proliferation. The cell number was assessed 3 days after plating. In the case of wild type cells, the number was approximately 80% greater for those treated with PDGF than for those not treated with PDGF. In the case of SM-MIRO1$^{-/-}$ VSMCs, cell counts were lower in both the PDGF-treated and non-treated cells, particularly in the former (**Figure S4A**).

Given the generally poor proliferation of VSMCs from SM-MIRO1$^{-/-}$ mice, in later experiments we used VSMCs isolated from MIRO1$^{fl/fl}$ mice and infected them with adenovirus expressing cre (Ad Cre; these cells are henceforth denoted as Miro1$^{-/-}$). As negative controls, we used cells isolated from the same mice infected with an empty vector control adenovirus (Ad EV). In this model, cre recombination was efficient (**Figure 2A, Figure S4B-D**). At 72 hr after plating in growth medium, the number of Miro1$^{-/-}$ VSMCs was significantly lower than that of wild type cells, both when the cells were grown under the same conditions and when they were additionally treated with PDGF (**Figure 2B**). Cells were synchronized by serum starvation for 48 hr and FACS analysis was performed to identify the phase of the cell cycle during which the growth delay caused by a lack of MIRO1 occurred (**Figure 2C-F, Figure S5**). At baseline (0 hr), no differences in the cell cycle distribution were observed across the experimental groups (**Figure 2D**). At both 24 h and 48 h, significant differences in percentage of cells in G1 and S phase were present. At 24 h, however, significantly more wild type than MIRO$^{-/-}$ VSMCs had exited the G1 phase. At 48 h, the percentage of wildtype cells in G1 was more than 80%, similar to the percentage at 0h, suggesting that the cell cycle was completed. In contrast, at 48 h, more MIRO1$^{-/-}$ VSMCs remained in S phase and fewer were in G1 phase than at 0h, indicating a delay in cell cycle (**Figure 2D-F, Figure S5**).

Immunoblotting for cyclin D1 and cyclin E in VSMCs incubated in serum-containing growth media for 24 h revealed significant decreases in the G1 phase and in the G1/S transition in MIRO1$^{-/-}$ VSMCs (**Figure 2G-I**), consistent with the results of the FACS analysis.

**MIRO1's EF hands are required for mitochondrial mobility and cell proliferation.**

Next, we also tested the extent to which the reconstitution of MIRO1 in MIRO1$^{-/-}$ VSMCs rescued cell proliferation. Expressing wildtype MIRO1 at levels similar to those in wild type cells normalized proliferation, whereas expressing a MIRO1 mutant lacking the EF hands at same levels only partially rescued cell proliferation (**Figure 3A-C**). These data demonstrate that MIRO1 is required for cell proliferation, that it affects early cell cycle progression during G1/S-phase, and that the EF hands of MIRO1 are necessary for normal cell proliferation.

The EF hands of MIRO1 mediate the attachment to microtubules in neurons and without them, mitochondria do not move normally within axons [13]. To determine the extent to which MIRO1 contributes to mitochondrial mobility in VSMCs, we plated wild type or MIRO1$^{-/-}$ VSMCs on microchips (CYTOOchip$^{TM}$) with Y-patterns. In wild type VSMCs, after cell cycle arrest caused by serum starvation, the mitochondria were concentrated around the nucleus. At 6 hr after treatment in growth media supplemented with PDGF, the mitochondria were distributed throughout the cell, including near the cell edges (**Figure 3D-F**). In the MIRO1$^{-/-}$ VSMCs, however, the mitochondria remained near the nucleus. Reconstitution of MIRO1$^{-/-}$ VSMCs with wild type MIRO1 fully rescued the mitochondrial distribution at 6 hr after PDGF treatment (**Figure 3G-J**). In contrast, after transduction of MIRO1$^{-/-}$ VSMCs with the MIRO1 mutant KK (MIRO1-KK), which lacks functional EF hands, the mitochondria were irregularly and unequally distributed. These data demonstrate that MIRO1 is required for both cell proliferation and coordinated mitochondrial mobility within the cell. In the absence of EF hands, proliferation and mobility is partially recovered, suggesting that MIRO1 supports proliferation through a mechanism beyond control of mobility.

Next, we sought to further elucidate the relationship of ATP production, mitochondrial mobility and VSMC proliferation. First, we determined whether mitochondrial ATP production is necessary for mitochondrial mobility or VSMC proliferation. For this purpose, we added

oligomycin, an inhibitor of ATP synthesis, to proliferating wild type VSMCs for 72 hr. This treatment reduced the number of VSMCs (**Figure 4A**) as well as in the intracellular ATP level (**Figure 4B**). To test the effect of ATP production by mitochondria on their mobility, we assessed the mitochondrial distribution in wild type VSMCs plated on micropatterned CYTOOchips. Mitochondrial mobility was reduced when ATP production was inhibited by oligomycin (**Figure 4C-E**). Then, to investigate whether blocking mitochondrial mobility affects intracellular ATP levels, we performed control experiments with Nocodazole, which inhibits microtubule assembly. This treatment effectively arrested mitochondrial mobility, but ATP levels were not affected (**Figure 4F, G).** These findings support that mitochondrial respiration is required for VSMC proliferation as well as mitochondrial mobility along microtubules and that MIRO1 controls both. In contrast, mitochondrial mobility is not required for optimal ATP production.

**Loss of MIRO1 leads to impaired metabolic activity and reduced proliferative capacity.** Our findings that mitochondrial mobility is controlled by MIRO1 and depends on mitochondrial ATP production imply that Miro1 deletion causes a defect in metabolic activity. Given cell proliferation is impaired at the early stages of the cell cycle in VSMCs with MIRO1 deletion and that intracellular ATP demands are high during the G1/S transition [28,29], we measured intracellular ATP levels in cells after 16 hr of PDGF treatment (**Figure 5A).** ATP levels were significantly lower in MIRO1$^{-/-}$ VSMCs than in their wild type counterparts. Additionally, transduction with MIRO1-WT normalized ATP production, whereas transduction with MIRO1-KK did not (**Figure 5B**). AMP kinase is an intracellular indicator of the metabolic state and regulates the expression of cyclins D and E. Thus, we determined AMP kinase activation by immunoblotting. In MIRO1$^{-/-}$ VSMCs, the phosphorylation of AMP kinase was elevated, indicating an intracellular energy deficiency (**Figure 5C-E**). AMP kinase suppresses cell cycle progression through phosphorylation and stabilization of p53 and subsequent induction of the p21, which leads to cell cycle arrest in G1 phase. In MIRO1-/- VSMCs, the p53 and p21 levels

increased and cyclin D1 decreased (**Figure 5F-H**), supporting that MIRO1 is required for energy production and cell-cycle progression in the G1/S phase. We also measured the oxygen consumption rate in wildtype and Miro1$^{-/-}$ VSMCs by Seahorse. We detected decreased basal respiration in MIRO1$^{-/-}$ VSMCs treated with PDGF compared to wild type (**Figure 5I, J**). However, the rate of extracellular acidification, a measure of glycolysis, was not significantly affected in MIRO1$^{-/-}$ VSMCs (**Figure 5K**), indicating a lack of compensatory upregulation of glycolysis.

**MIRO1 controls electron transport chain (ETC) activity**

We sought to establish the mechanism by which MIRO1 controls ATP production. Previous findings in embryonic fibroblasts have suggested that MIRO1 associates with both the mitochondrial contact site (MICOS) complex and the mitochondrial intermembrane space bridging (MIB) complex, which collectively control the folding of mitochondrial cristae [21]. Moreover, we recently reported that MIRO1 regulates the formation of mitochondria-ER contact sides (MERCS) during the cell cycle and facilitates the $Ca^{2+}$ transfer to mitochondria. We assessed the effect of MIRO1 deletion on the formation of mitochondrial cristae in VSMCs by transmission electron microscopy. Consistent with findings in fibroblasts [21], we found that in Miro1$^{-/-}$ VSMCs, the cristae were less dense than those in wild type controls, and their morphology was distorted (**Figure 6A-C**). Next, we established the associations of wild type MIRO1, MIRO1-KK, and a MIRO1 mutant lacking the C-terminal transmembrane domain with components of the electron transport chain and the MIB/MICOS complex. Pull-down experiments in HEK 293T cells revealed interactions between MIRO1 and several MIB/MICOS proteins (Sam50, Mic60, and Mic19; **Figure 6D-G**) and NDUFA9 subunits of electron transport chain complex I (**Figure 6H).** The transmembrane domain by which MIRO1 is attached to mitochondria was necessary for the association with all proteins, and in the absence of the EF

hands the association with all proteins was weaker. The expression of proteins of the MIB/MICOS complex was not affected by MIRO1 deletion (**Figure S6A**).

In the case of the ETC complexes, immunoblotting for subunits of all five electron transport chain complexes was evaluated, but this did not reveal a significant difference in protein levels between wild type and MIRO1$^{-/-}$ VSMCs (**Figure S6B-G**). Because the formation of mitochondrial cristae affects the formation of the MIB/MICOS super complex and the activity of the ETC chain, we tested the abundance of mitochondrial super complexes in blue native gels (**Figure 6I, J**). The levels of super complex II were decreased in MIRO1$^{-/-}$ VSMCs compared wild type VSMCs (**Figure 6J**). We also tested the activity of ETC complex I by measuring the consumption of NADH. In MIRO1$^{-/-}$ cells, the activity of this complex was significantly decreased (**Figure 6K, L**). These data demonstrate that MIRO1 associates with MIB/MICOS and that this interaction promotes the formation of mitochondrial super complexes and the activity of ETC complex I.

**MIRO1 knockdown in human coronary smooth muscle cells impairs proliferation, mitochondrial mobility, and ETC activity.**

To determine if these findings also apply to human cells, MIRO1 was knocked down in human coronary smooth muscle cells (**Figure 7A, B**). Cell counts 72 hours after plating revealed a significant decrease in the number of cells with MIRO1 knockdown, particularly in those treated with PDGF (**Figure 7C**). Additionally, in VSMCs plated on microchips (CYTOOchipTM) with Y-patterns and treated with PDGF, MIRO1 knockdown led to a concentration of mitochondria near the nucleus, similar to mouse MIRO-/- VSMCs. In control conditions, the mitochondria were distributed throughout the cell, including near the edges (**Figure 7D-F**). The intracellular ATP levels were reduced with MIRO1 knockdown (**Figure 7G, H**). Finally, the activity of ETC complex I, measured by NADH consumption, was significantly decreased in MIRO1$^{-/-}$ cells

(**Figure 7I, J**). These results indicate that the effects of MIRO1 on proliferation and metabolism in VSMCs are conserved among species and potentially clinically relevant for human disease.

**Pharmacological reduction of MIRO1 impairs VSMC proliferation**

Finally, we tested whether the pharmacological reduction in MIRO1 yields effects on cell proliferation and ATP production similar to those observed with the genetic deletion of the protein. Recently, a small-molecule MIRO1 reducer [20] was developed that removes MIRO1 specifically from mitochondria, leading to the loss of mitochondria through increased mitophagy. In wild type VSMCs, incubation with this compound for 72 h reduced mitochondrial mass (**Figure S7A-C**). It also decreased the number of proliferating VSMCs at 72 hr (**Figure S7D**). The effect of the reducer on cell number was dose-dependent (**Figure S7E**). Furthermore, the compound also lowered intracellular ATP levels in wild type VSMCs (**Figure S7F**). These findings suggest that reducing MIRO1 could be utilized to treat vasoproliferative diseases, such as neointima formation.

## DISCUSSION

This study uncovers the crucial role of the outer mitochondrial membrane GTPase, MIRO1, in driving VSMC proliferation and neointima formation. The findings highlight that mitochondrial mobility, regulated by MIRO1, is essential not only for cell migration, as previously established [15,30], but also for smooth muscle cell proliferation. Contrary to the belief that mitochondrial mobility is mainly required to align mitochondria before mitosis, the study demonstrates that proliferation is hindered in the early cell cycle stages, particularly during the ATP-demanding G1 to S phase transition.

The research shows that MIRO1$^{-/-}$ cells have reduced ATP levels, emphasizing the importance of MIRO1-mediated ATP production. Based on our recent report [25], we posit that mitochondrial mobility facilitates the formation of MERCS, which support enhanced calcium transfer during the G1 to S phase, ultimately boosting ATP production. Furthermore, MIRO1 forms associations with the MIB/MICOS complex, the microtubule motor machinery, and the ETC subunit Nduf9, suggesting a dual role in supporting both mitochondrial ATP production and mobility. This insight into the interplay between mitochondrial dynamics and cellular energy metabolism offers advancements in understanding mitochondrial function in proliferation mechanisms.

Firstly, we discovered that neointima formation is abolished in a mouse model with VSMC-specific MIRO1 deletion, and that cell proliferation in cultured aortic VSMCs lacking MIRO1 is significantly reduced due to delays in the early phases of the cell cycle. Unlike previous research primarily focusing on the role of MIRO1 in neurons and embryonic fibroblasts [16,19-21,31-35], our findings extend its importance to primary proliferating VSMCs, revealing its critical involvement in VSMC proliferation and neointima formation. We are the first to demonstrate that MIRO1 deletion in VSMCs results in abolished neointima formation in a mouse model, highlighting MIRO1 as a potential new therapeutic target for treating vasoproliferative diseases.

In immortalized cells lacking MIRO1 and 2[16], impaired cytokinesis with asymmetric partitioning of mitochondria to daughter cells was reported in M-phase [36]. In addition to reduced progression in the G2/M phase in MIRO1$^{-/-}$ VSMCs, we found strong evidence for impairments in the early phases of the cell cycle.

Secondly, the loss of MIRO1 reduced intracellular ATP levels and abolished mitochondrial mobility. Moreover, inhibiting mitochondrial respiration blocked their mobility, whereas halting mobility by microtubule disassembly did not affect ATP levels. MIRO1 not only controls mobility, but also supercomplex formation and ETC activity. Thus, we provide evidence on the relationship that mitochondrial energy production is required for mitochondrial mobility. Whether reduced ATP production negatively impacts mitochondrial mobility because of impaired activity of the C-terminal GTPase domain of MIRO1 as recently described or impaired actin polymerization will require further investigation [37].

VSMCs are believed to mostly rely on glycolysis to fuel their proliferation [38]. However, recent studies have provided evidence that, analogous to proliferating cancer cells, VSMCs also depend on glutaminolysis [39 40], which shuttles metabolites to the TCA cycle and promotes oxidative phosphorylation. Our findings indicate that VSMCs require mitochondrial ATP since ATP synthase inhibition blocked mitochondrial mobility and VSMC proliferation. In our study, halting mitochondrial mobility by microtubule disassembly did not decrease overall intracellular ATP levels in VSMCs. These data further support that mitochondrial mobility controlled by MIRO1 enables subcellular mitochondrial positioning within VSMCs, which then supports localized subcellular ATP and ROS production. MIRO1 ensures that mitochondrial metabolites exert their effects on local targets, similar to findings in embryonic fibroblasts [41,42].

Thirdly, we found that the reconstitution of MIRO1$^{-/-}$ VSMCs with MIRO1-WT normalized cell proliferation, ATP levels, and mobility, whereas the reconstitution of MIRO1-KK, which lacks EF hands, resulted in only partial recovery. These results suggest that the EF hands of MIRO1 are important for its full functionality in VSMCs. In neurons, MIRO1 regulates the anterograde transport of mitochondria along microtubules [16,43,44]. Mitochondrial arrest in response to elevated $Ca^{2+}$ in subcellular domains and synaptic activity is driven by the $Ca^{2+}$-sensing EF hands [32,45]. Here, we provide evidence that without $Ca^{2+}$-controlled mitochondrial arrest through point mutations of the EF hands, VSMC proliferation is reduced. We speculate that the loss of functional EF hands impairs alignment of mitochondria and ER. In a recent study, we demonstrated that MIRO1 deficiency disrupts MERCS formation and mitochondrial calcium uptake during the cell cycle [25].

Fourthly, MIRO1 loss caused an intracellular energy deficit, increased AMP kinase phosphorylation, and reduced the expression of proteins promoting the G1/S cell-cycle transition. This finding suggests a mechanism where MIRO1 influences cell proliferation through its impact on cellular energy status and cell cycle regulatory proteins. Indeed, a link between AMP kinase activation and upregulation of p53 and G1/S cell cycle arrest has been described [28,46]. Here, our data provide an explanation for how low ATP levels caused by MIRO1 deletion block cell cycle progression at this cell cycle stage.

Fifth, we observed that MIRO1 loss impaired the formation of mitochondrial cristae as observed in embryonic fibroblasts [21]. In our model of VSMCs with MIRO1 deletion, this correlated with reduced formation of ETC supercomplexes and activity of ETC complex I. In agreement with a prior study, MIRO1 associated with MIC19, MIC60 and SAM50 and the expression of MICOS/MIB proteins were not impaired with MIRO1 deletion [21]. In addition, we detected a previously unrecognized association between NDUFA9, a subunit of ETC complex I, and

decreased ETC complex I activity. These findings provide a potential mechanism by which MIRO1 controls mitochondrial ATP production, in addition to putative decreasing metabolite transfer at distorted mitochondrial ER contact sites [16,21,25] .

Some findings of our study agree with published data on MIRO1, which have highlighted its role in mitochondrial dynamics, energy production, and cell signaling. Previous studies have shown that MIRO1 is involved in the regulation of mitochondrial transport and positioning, which are critical for metabolic signaling [13,15,41,47]. The observed effects of MIRO1 loss on ATP production and mitochondrial structure in our study align with reports indicating that MIRO1 dysfunction can lead to impaired mitochondrial respiration and energy deficits [15,21,41,44]. Additionally, the role of MIRO1 in cell proliferation is supported by the literature demonstrating its involvement in mitotic spindle formation at later stages of the cell cycle and most recently, also in G1/S phase [15,16,21].

Despite these compelling findings, our study has limitations. One limitation is the use of a mouse model, which, while informative, may not fully replicate human VSMC behavior. We selected the complete ligation model for this study due to its high reproducibility and excellent surgical feasibility [27], which allow for consistent outcomes across investigators. While it does not fully replicate some aspects of human balloon angioplasty with restenosis, such as endothelial denudation, it provides valuable insights into mechanisms of neointima formation. Additionally, our experiments focused primarily on cultured aortic VSMCs, which may not entirely represent the in vivo environment. Future studies should include a broader range of VSMC models and in vivo validations to confirm these mechanisms. Moreover, MIRO1 shares 60% sequence identity with its paralog MIRO2 [31]. Both are ubiquitously expressed in eukaryotes, yet they are not functionally redundant [16,44]. In VSMCs with MIRO1 deletion, we did not detect a compensatory upregulation of MIRO2. The functions of MIRO2 in the vasculature are currently unknown.

However, a previous study proposed that after trans-aortic banding, the expression of MIRO2 in cardiac myocytes improved mitochondrial function [48].

In conclusion, our study demonstrated that MIRO1 is a pivotal regulator of VSMC proliferation and neointima formation. Our study revealed the specific mechanisms by which MIRO1 regulates ATP production and mitochondrial mobility, linking these processes to cell cycle progression and energy homeostasis. This connection between mitochondrial dynamics and cell proliferation is a significant advancement in understanding how mitochondrial dysfunction can contribute to vascular disease.  The findings suggest that targeting MIRO1 could be a potential therapeutic strategy for treating vasoproliferative diseases, such as neointima formation. Further research is needed to fully understand the downstream effects of MIRO1 loss and to explore the potential clinical applications of these insights.

**Acknowledgements:** The authors thank Dr. Christine Blaumueller of the Scientific Editing and Research Communication Core at the University of Iowa Carver College of Medicine for critical reading of the manuscript.

**Sources of Funding:** This project was supported by grants from the NIH (R01 HL 108932 to IMG and R01 HL 157956 to IMG and WHT); the Department of Veterans Affairs (I01 BX000163 to IMG); and the American Heart Association (17GRNT33660032 to IMG and 22PRE902649 to BTE). The contents of this article do not represent the views of the Department of Veterans Affairs or the US Government.

## REFERENCES


1. Ballinger SW. Mitochondrial dysfunction in cardiovascular disease. *Free Radic Biol Med*. 2005;38:1278-1295. doi: 10.1016/j.freeradbiomed.2005.02.014
2. Wang Y, Tabas I. Emerging roles of mitochondria ROS in atherosclerotic lesions: causation or association? *J Atheroscler Thromb*. 2014;21:381-390.
3. Deuse T, Hua X, Wang D, Maegdefessel L, Heeren J, Scheja L, Bolanos JP, Rakovic A, Spin JM, Stubbendorff M, et al. Dichloroacetate prevents restenosis in preclinical animal models of vessel injury. *Nature*. 2014;509:641-644. doi: 10.1038/nature13232
4. Lv L, Meng Q, Ye M, Wang P, Xue G. STAT4 deficiency protects against neointima formation following arterial injury in mice. *J Mol Cell Cardiol*. 2014;74:284-294. doi: 10.1016/j.yjmcc.2014.06.001
5. Guo X, Chen KH, Guo Y, Liao H, Tang J, Xiao RP. Mitofusin 2 triggers vascular smooth muscle cell apoptosis via mitochondrial death pathway. *Circ Res*. 2007;101:1113-1122. doi: 10.1161/CIRCRESAHA.107.157644
6. Vendrov AE, Vendrov KC, Smith A, Yuan J, Sumida A, Robidoux J, Runge MS, Madamanchi NR. NOX4 NADPH Oxidase-Dependent Mitochondrial Oxidative Stress in Aging-Associated Cardiovascular Disease. *Antioxid Redox Signal*. 2015. doi: 10.1089/ars.2014.6221
7. Wang JN, Shi N, Chen SY. Manganese superoxide dismutase inhibits neointima formation through attenuation of migration and proliferation of vascular smooth muscle cells. *Free radical biology & medicine*. 2012;52:173-181. doi: 10.1016/j.freeradbiomed.2011.10.442 [doi]
8. Zhang Y, Li W, Wang P, Gu R, Feng Y, Wei S, Peng K, Su L, Wang Q, Li, et al. Uncoupling Protein 2 Inhibits Myointimal Hyperplasia in Preclinical Animal Models of Vascular Injury. *J Am Heart Assoc*. 2017;6. doi: 10.1161/JAHA.117.006593
9. Wang L, Yu T, Lee H, O'Brien DK, Sesaki H, Yoon Y. Decreasing mitochondrial fission diminishes vascular smooth muscle cell migration and ameliorates intimal hyperplasia. *Cardiovasc Res*. 2015;106:272-283. doi: 10.1093/cvr/cvv005
10. Lim S, Lee SY, Seo HH, Ham O, Lee C, Park JH, Lee J, Seung M, Yun I, Han SM, et al. Regulation of mitochondrial morphology by positive feedback interaction between PKCdelta and Drp1 in vascular smooth muscle cell. *J Cell Biochem*. 2015;116:648-660. doi: 10.1002/jcb.25016
11. Umezu R, Koga JI, Matoba T, Katsuki S, Wang L, Hasuzawa N, Nomura M, Tsutsui H, Egashira K. Macrophage (Drp1) Dynamin-Related Protein 1 Accelerates Intimal Thickening After Vascular Injury. *Arterioscler Thromb Vasc Biol*. 2020;40:e214-e226. doi: 10.1161/ATVBAHA.120.314383
12. Chalmers S, Saunter C, Wilson C, Coats P, Girkin JM, McCarron JG. Mitochondrial motility and vascular smooth muscle proliferation. *Arterioscler Thromb Vasc Biol*. 2012;32:3000-3011. doi: 10.1161/ATVBAHA.112.255174
13. Wang X, Schwarz TL. The mechanism of Ca2+ -dependent regulation of kinesin-mediated mitochondrial motility. *Cell*. 2009;136:163-174. doi: 10.1016/j.cell.2008.11.046
14. Morlino G, Barreiro O, Baixauli F, Robles-Valero J, Gonzalez-Granado JM, Villa-Bellosta R, Cuenca J, Sanchez-Sorzano CO, Veiga E, Martin-Cofreces NB, et al. Miro-1 links mitochondria and microtubule Dynein motors to control lymphocyte migration and polarity. *Mol Cell Biol*. 2014;34:1412-1426. doi: 10.1128/MCB.01177-13
15. Schuler MH, Lewandowska A, Caprio GD, Skillern W, Upadhyayula S, Kirchhausen T, Shaw JM, Cunniff B. Miro1-mediated mitochondrial positioning shapes intracellular energy gradients required for cell migration. *Mol Biol Cell*. 2017;28:2159-2169. doi: 10.1091/mbc.E16-10-0741

16. Lopez-Domenech G, Covill-Cooke C, Ivankovic D, Halff EF, Sheehan DF, Norkett R, Birsa N, Kittler JT. Miro proteins coordinate microtubule- and actin-dependent mitochondrial transport and distribution. *EMBO J*. 2018;37:321-336. doi: 10.15252/embj.201696380
17. Fransson S, Ruusala A, Aspenstrom P. The atypical Rho GTPases Miro-1 and Miro-2 have essential roles in mitochondrial trafficking. *Biochem Biophys Res Commun*. 2006;344:500-510. doi: 10.1016/j.bbrc.2006.03.163
18. Oeding SJ, Majstrowicz K, Hu XP, Schwarz V, Freitag A, Honnert U, Nikolaus P, Bahler M. Identification of Miro1 and Miro2 as mitochondrial receptors for myosin XIX. *J Cell Sci*. 2018;131. doi: 10.1242/jcs.219469
19. Safiulina D, Kuum M, Choubey V, Gogichaishvili N, Liiv J, Hickey MA, Cagalinec M, Mandel M, Zeb A, Liiv M, et al. Miro proteins prime mitochondria for Parkin translocation and mitophagy. *EMBO J*. 2019;38. doi: 10.15252/embj.201899384
20. Hsieh CH, Li L, Vanhauwaert R, Nguyen KT, Davis MD, Bu G, Wszolek ZK, Wang X. Miro1 Marks Parkinson's Disease Subset and Miro1 Reducer Rescues Neuron Loss in Parkinson's Models. *Cell Metab*. 2019;30:1131-1140 e1137. doi: 10.1016/j.cmet.2019.08.023
21. Modi S, Lopez-Domenech G, Halff EF, Covill-Cooke C, Ivankovic D, Melandri D, Arancibia-Carcamo IL, Burden JJ, Lowe AR, Kittler JT. Miro clusters regulate ER-mitochondria contact sites and link cristae organization to the mitochondrial transport machinery. *Nat Commun*. 2019;10:4399. doi: 10.1038/s41467-019-12382-4
22. Chemla A, Arena G, Onal G, Walter J, Berenguer-Escuder C, Grossmann D, Grünewald A, Schwamborn JC, Krüger R. Generation of two induced pluripotent stem cell lines and the corresponding isogenic controls from Parkinson's disease patients carrying the heterozygous mutations c.815G > A (p.R272Q) or c.1348C > T (p.R450C) in the RHOT1 gene encoding Miro1. *Stem Cell Res*. 2023;71:103145. doi: 10.1016/j.scr.2023.103145
23. Conejeros C, Parra V, Sanchez G, Pedrozo Z, Olmedo I. Miro1 as a novel regulator of hypertrophy in neonatal rat cardiomyocytes. *J Mol Cell Cardiol*. 2020;141:65-69. doi: 10.1016/j.yjmcc.2020.03.014
24. Koval OM, Nguyen EK, Santhana V, Fidler TP, Sebag SC, Rasmussen TP, Mittauer DJ, Strack S, Goswami PC, Abel ED, et al. Loss of MCU prevents mitochondrial fusion in G1-S phase and blocks cell cycle progression and proliferation. *Sci Signal*. 2019;12. doi: 10.1126/scisignal.aav1439
25. Endoni BT, Koval OM, Allamargot C, Kortlever T, Qian L, Sadoski RJ, Juhr D, Grumbach IM. MIRO1 Is Required for Dynamic Increases in Mitochondria-ER Contact Sites and Mitochondrial ATP During the Cell Cycle. *Cells*. 2025;14. doi: 10.3390/cells14070482
26. Shannon N, Raymond C, Palmer C, Homa S, Bonini M, Seward D, Cunniff B. Miro1 expression alters global gene expression, ERK1/2 phosphorylation, oxidation and cell cycle progression. *J Cell Sci*. 2025;138. doi: 10.1242/jcs.263554
27. Kumar A, Lindner V. Remodeling with neointima formation in the mouse carotid artery after cessation of blood flow. *Arteriosclerosis, Thrombosis, and Vascular Biology*. 1997;17:2238-2244.
28. Mitra K, Wunder C, Roysam B, Lin G, Lippincott-Schwartz J. A hyperfused mitochondrial state achieved at G1-S regulates cyclin E buildup and entry into S phase. *Proc Natl Acad Sci U S A*. 2009;106:11960-11965. doi: 10.1073/pnas.0904875106
29. Montemurro C, Vadrevu S, Gurlo T, Butler AE, Vongbunyong KE, Petcherski A, Shirihai OS, Satin LS, Braas D, Butler PC, et al. Cell cycle-related metabolism and mitochondrial dynamics in a replication-competent pancreatic beta-cell line. *Cell Cycle*. 2017;16:2086-2099. doi: 10.1080/15384101.2017.1361069
30. Nguyen EK, Koval OM, Noble P, Broadhurst K, Allamargot C, Wu M, Strack S, Thiel WH, Grumbach IM. CaMKII (Ca 2+ /Calmodulin-Dependent Kinase II) in Mitochondria of

Smooth Muscle Cells Controls Mitochondrial Mobility, Migration, and Neointima Formation. *Arterioscler Thromb Vasc Biol*. 2018. doi: 10.1161/ATVBAHA.118.310951
31. Birsa N, Norkett R, Higgs N, Lopez-Domenech G, Kittler JT. Mitochondrial trafficking in neurons and the role of the Miro family of GTPase proteins. *Biochem Soc Trans*. 2013;41:1525-1531. doi: 10.1042/BST20130234
32. Chang KT, Niescier RF, Min KT. Mitochondrial matrix Ca2+ as an intrinsic signal regulating mitochondrial motility in axons. *Proc Natl Acad Sci U S A*. 2011;108:15456-15461. doi: 10.1073/pnas.1106862108
33. Schwarz L, Sharma K, Dodi LD, Rieder LS, Fallier-Becker P, Casadei N, Fitzgerald JC. Miro1 R272Q disrupts mitochondrial calcium handling and neurotransmitter uptake in dopaminergic neurons. *Front Mol Neurosci*. 2022;15:966209. doi: 10.3389/fnmol.2022.966209
34. Niescier RF, Hong K, Park D, Min KT. MCU Interacts with Miro1 to Modulate Mitochondrial Functions in Neurons. *J Neurosci*. 2018;38:4666-4677. doi: 10.1523/JNEUROSCI.0504-18.2018
35. Castro IG, Richards DM, Metz J, Costello JL, Passmore JB, Schrader TA, Gouveia A, Ribeiro D, Schrader M. A role for Mitochondrial Rho GTPase 1 (MIRO1) in motility and membrane dynamics of peroxisomes. *Traffic*. 2018;19:229-242. doi: 10.1111/tra.12549
36. Kanfer G, Courtheoux T, Peterka M, Meier S, Soste M, Melnik A, Reis K, Aspenstrom P, Peter M, Picotti P, et al. Mitotic redistribution of the mitochondrial network by Miro and Cenp-F. *Nat Commun*. 2015;6:8015. doi: 10.1038/ncomms9015
37. Peters DT, Kay L, Eswaran J, Lakey JH, Soundararajan M. Human Miro Proteins Act as NTP Hydrolases through a Novel, Non-Canonical Catalytic Mechanism. *Int J Mol Sci*. 2018;19. doi: 10.3390/ijms19123839
38. Perez J, Hill BG, Benavides GA, Dranka BP, Darley-Usmar VM. Role of cellular bioenergetics in smooth muscle cell proliferation induced by platelet-derived growth factor. *Biochem J*. 2010;428:255-267. doi: 10.1042/BJ20100090
39. Zhang CY, Hu YC, Zhang Y, Ma WD, Song YF, Quan XH, Guo X, Wang CX. Glutamine switches vascular smooth muscle cells to synthetic phenotype through inhibiting miR-143 expression and upregulating THY1 expression. *Life Sci*. 2021:119365. doi: 10.1016/j.lfs.2021.119365
40. Park HY, Kim MJ, Lee S, Jin J, Kim JG, Choi YK, Park KG. Inhibitory Effect of a Glutamine Antagonist on Proliferation and Migration of VSMCs via Simultaneous Attenuation of Glycolysis and Oxidative Phosphorylation. *Int J Mol Sci*. 2021;22. doi: 10.3390/ijms22115602
41. Alshaabi H, Shannon N, Gravelle R, Milczarek S, Messier T, Cunniff B. Miro1-mediated mitochondrial positioning supports subcellular redox status. *Redox Biol*. 2021;38:101818. doi: 10.1016/j.redox.2020.101818
42. Alshaabi H, Heininger M, Cunniff B. Dynamic regulation of subcellular mitochondrial position for localized metabolite levels. *J Biochem*. 2020;167:109-117. doi: 10.1093/jb/mvz058
43. Moller A, Bauer CS, Cohen RN, Webster CP, De Vos KJ. Amyotrophic lateral sclerosis-associated mutant SOD1 inhibits anterograde axonal transport of mitochondria by reducing Miro1 levels. *Hum Mol Genet*. 2017;26:4668-4679. doi: 10.1093/hmg/ddx348
44. Nguyen TT, Oh SS, Weaver D, Lewandowska A, Maxfield D, Schuler MH, Smith NK, Macfarlane J, Saunders G, Palmer CA, et al. Loss of Miro1-directed mitochondrial movement results in a novel murine model for neuron disease. *Proc Natl Acad Sci U S A*. 2014;111:E3631-3640. doi: 10.1073/pnas.1402449111
45. Macaskill AF, Rinholm JE, Twelvetrees AE, Arancibia-Carcamo IL, Muir J, Fransson A, Aspenstrom P, Attwell D, Kittler JT. Miro1 is a calcium sensor for glutamate receptor-

dependent localization of mitochondria at synapses. *Neuron*. 2009;61:541-555. doi: 10.1016/j.neuron.2009.01.030

46. Finkel T, Hwang PM. The Krebs cycle meets the cell cycle: mitochondria and the G1-S transition. *Proc Natl Acad Sci U S A*. 2009;106:11825-11826. doi: 10.1073/pnas.0906430106

47. Stephen TL, Higgs NF, Sheehan DF, Al Awabdh S, Lopez-Domenech G, Arancibia-Carcamo IL, Kittler JT. Miro1 Regulates Activity-Driven Positioning of Mitochondria within Astrocytic Processes Apposed to Synapses to Regulate Intracellular Calcium Signaling. *J Neurosci*. 2015;35:15996-16011. doi: 10.1523/JNEUROSCI.2068-15.2015

48. Cao Y, Xu C, Ye J, He Q, Zhang X, Jia S, Qiao X, Zhang C, Liu R, Weng L, et al. Miro2 Regulates Inter-Mitochondrial Communication in the Heart and Protects Against TAC-Induced Cardiac Dysfunction. *Circ Res*. 2019;125:728-743. doi: 10.1161/CIRCRESAHA.119.315432

Figure 1

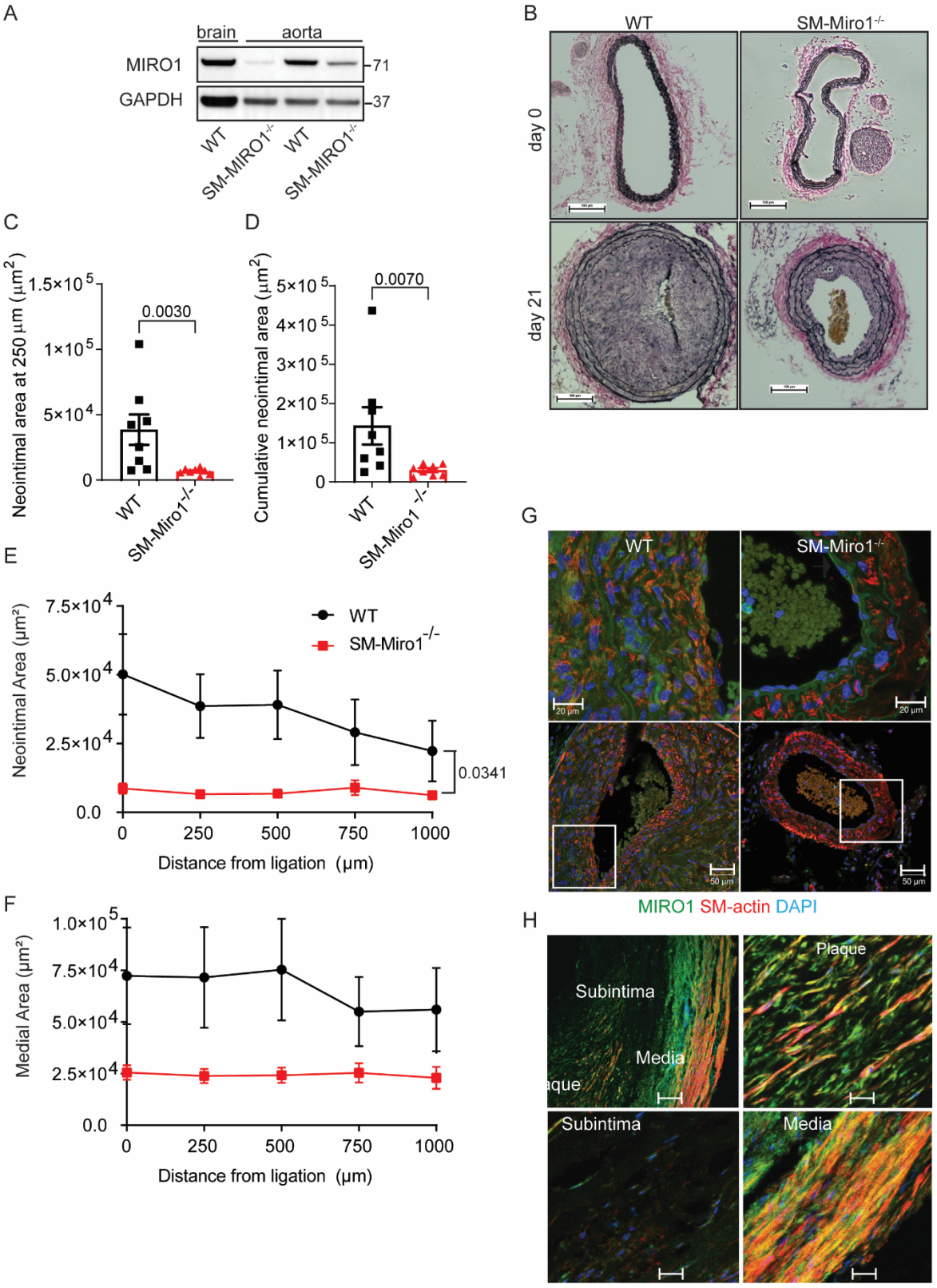
A
brain
aorta
MIRO1
GAPDH
71
37
WT
SM-MIRO1-/-
WT
SM-MIRO1-/-
B
WT
SM-Miro1-/-
day 0
day 21
C
Neointimal area at 250 µm (µm2)
1.5×10 5
1×10 5
5×10 4
0
0.0030
WT
SM-Miro1-/-
D
Cumulative neointimal area (µm2)
5×10 5
4×10 5
3×10 5
2×10 5
1×10 5
0
0.0070
WT
SM-Miro1 -/-
E
Neointimal Area (µm2)
7.5×10 4
5.0×10 4
2.5×10 4
0.0
WT
SM-Miro1-/-
0.0341
0
250
500
750
1000
Distance from ligation (µm)
F
Medial Area (µm2)
1.0×10 5
7.5×10 4
5.0×10 4
2.5×10 4
0.0
0
250
500
750
1000
Distance from ligation (µm)
G
WT
SM-Miro1-/-
20 µm
20 µm
50 µm
50 µm
MIRO1 SM-actin DAPI
H
Subintima
Media
Plaque
Subintima
Media

**Figure 1. Loss of Miro1 blocks neointima formation.**

(**A**) Immunoblots for MIRO1 in lysates from brain and aorta isolated from WT and SM-Miro1$^{-/-}$ mice.
(**B**) Verhoeff-Van Gieson staining in the unligated and ligated common carotid arteries of wild type and SM-Miro1$^{-/-}$ mice, at 21 days post ligation. Scale bar = 100 µm.
(**C**) Neointimal area in ligated carotid arteries at 250 µm from the bifurcation. Neointimal area was determined by subtracting the luminal area from the area defined by the internal elastic lamina.
(**D**) Cumulative neointimal area, calculated from all neointimal areas within 1000 µm of the bifurcation.
(**E**) Neointimal area at the indicated distances from the site of ligation.
(**F**) Medial area at the indicated distances from the site of ligation. The medial area was determined by subtracting the area defined by the internal elastic lamina from the area defined by the external elastic lamina.
(**G**) Immunofluorescence of MIRO1 expression in the mouse carotid artery. MIRO1, green; SM-actin, red; DAPI, blue. Scale bar: 20 µm in upper images; 50 µm in lower images. Upper images are magnifications of the areas labeled with a box in the lower images.
(**H**) Immunofluorescence of MIRO1 in the left anterior descending artery of a healthy subject and that of a patient with coronary artery disease. MIRO1, green; SM-actin, red; DAPI, blue. Scale bar: 80 µm in upper, 20 µm in lower images.
Statistical analyses were performed using Mann-Whitney test (C, D) and two-way ANOVA (E, F).

Figure 2

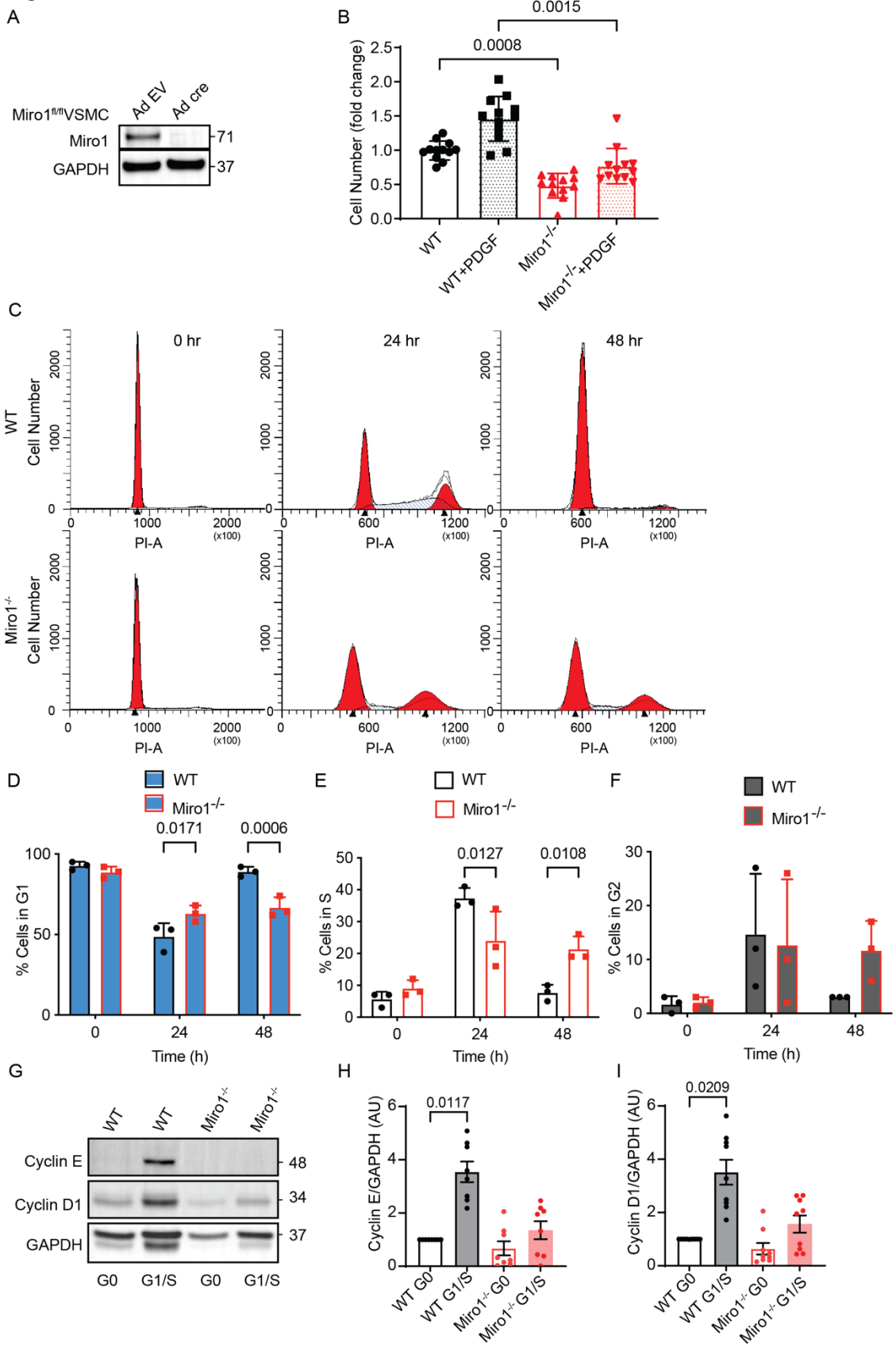
A
Miro1fl/flVSMC
Ad EV
Ad cre
Miro1
GAPDH
71
37
B
0.0015
0.0008
Cell Number (fold change)
WT
WT+PDGF
Miro1-/-
Miro1-/-+PDGF
C
0 hr
24 hr
48 hr
WT
Miro1-/-
Cell Number
PI-A
(x100)
D
WT
Miro1-/-
0.0171
0.0006
% Cells in G1
Time (h)
E
0.0127
0.0108
% Cells in S
F
% Cells in G2
G
Cyclin E
Cyclin D1
GAPDH
48
34
37
G0
G1/S
H
0.0117
Cyclin E/GAPDH (AU)
WT G0
WT G1/S
Miro1-/- G0
Miro1-/- G1/S
I
0.0209
Cyclin D1/GAPDH (AU)

**Figure 2. Loss of Miro1 reduces G1/S transition and VSMC proliferation.**

(**A**) MIRO1 levels in mitochondrial fractions of VSMCs from Miro1$^{fl/fl}$ mice transduced with adenovirus expressing Cre or control adenovirus, as determined by immunoblotting.
(**B**) Number of VSMCs from Miro1$^{fl/fl}$ mice following transduction with adenovirus expressing cre (MIRO1$^{-/-}$) or control (WT) adenovirus, at 72 hr after incubation with PDGF (20 ng/ml) or control (saline).
(**C**) DNA content of synchronized WT and MIRO1$^{-/-}$ VSMCs, as assessed by fluorescence-activated cell sorting (FACS). Times are 0, 24, and 48 hr after release from growth arrest for 48h in FBS-free media, and then at 24 and 48 hr after release from arrest with media containing 10% FBS. Analysis compared differences between genotypes.
(**D-F**) Quantification of cell-cycle phase distribution of WT and MIRO1$^{-/-}$ VSMCs shown in C.
(**G**) Immunoblots for cyclin E and D1 as markers of the indicated cell cycle phases in whole-cell lysates of WT and Miro1$^{-/-}$ VSMCs following synchronization by serum starvation, at G0 (after growth arrest for 48 hr in FBS-free media), and G1/S (after release from growth arrest with media containing 10% FBS for 24 hr).
(**H, I**) Quantification of Cyclin D1 and E levels on immunoblots like those shown in panel G. Statistical analyses were performed using Kruskal-Wallis test (B) and two-way ANOVA (D-F), and Friedman test (H, I).

Figure 3

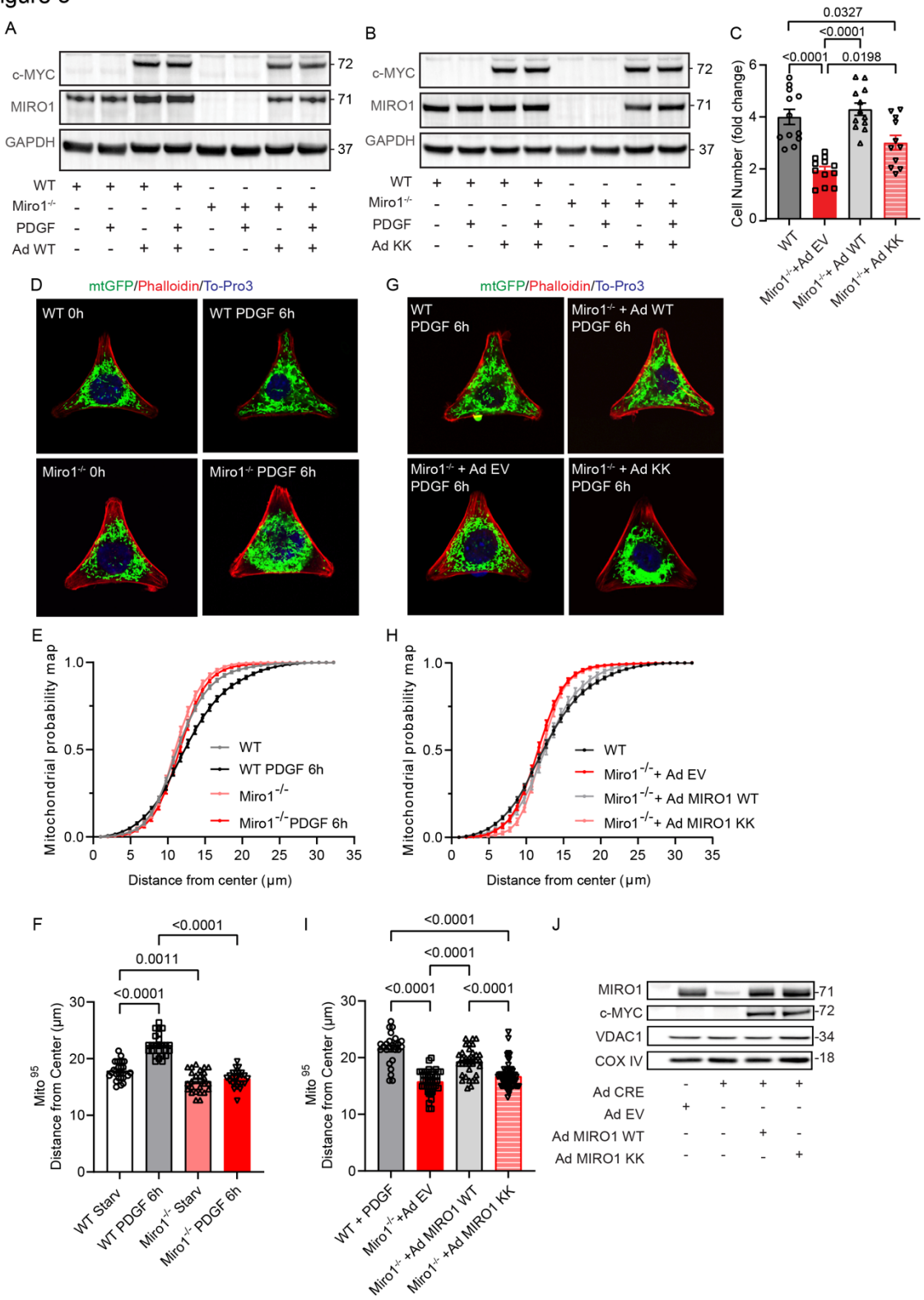


**Figure 3. Loss of EF hands in MIRO1 reduces mitochondrial mobility and cell proliferation.**

(**A, B**) Immunoblots for MIRO1 and c-MYC in WT and Miro1$^{-/-}$ VSMCs transduced with adenovirus expressing MIRO1-WT (A) and MIRO1-KK (A).
(**C**) Number of WT and Miro1 $^{-/-}$ VSMCs transduced with adenovirus expressing MIRO1-WT, MIRO1-KK, or control adenovirus (empty vector, Ad EV) and treated with PDGF (20 ng/ml) for 72 hr.
(**D**) Representative confocal images of WT and Miro1$^{-/-}$ VSMCs grown on Y-shaped adhesive micropatterns (CYTOOchips$^{TM}$), with VSMCs synchronized by serum starvation for 24 hr (0 hr timepoint), followed by change to medium containing 10% FCS and PDGF (20 ng/ml) for 6hr (Phalloidin, red; mitochondrial GFP, green; DAPI, blue).
(**E**) Mitochondrial probability map. The cumulative distribution of mitochondria was assessed for images as in (A) by modified Sholl's analysis. Data are plotted by growth conditions.
(**F**) Mito$^{95}$ values, defined as the distance from the center of the CYTOOchips$^{TM}$ at which 95% of the mitochondrial signal is found, under the conditions used in (A).
(**G**) Representative confocal images of WT and Miro1$^{-/-}$ VSMCs grown on CYTOOchips$^{TM}$. Miro1$^{-/-}$ VSMCs were transduced with adenovirus expressing MIRO1-WT or MIRO1-KK for 72 hr before being seeded onto CYTOOchips$^{TM}$. The cell cycle was synchronized by serum starvation for 24 hr (not shown); the cells were subsequently treated with medium containing 10% FCS and PDGF (20 ng/ml) for 6 hr.
(**H**) Mitochondrial probability map. The cumulative distribution of mitochondria was assessed for images shown in (D). Data are plotted as in B.
(**I**) Mito$^{95}$ values, as defined in (C) but under the conditions used in (D).
(**J**) Immunoblots for MIRO1 and c-myc in WT and Miro1$^{-/-}$ VSMCs transduced with adenoviruses expressing MIRO1-WT (Ad WT), MIRO1-KK (Ad KK), or with control adenovirus (empty vector; Ad EV).
Statistical analyses were performed by one-way ANOVA (C, F) and Kruskal-Wallis test (I).

Figure 4

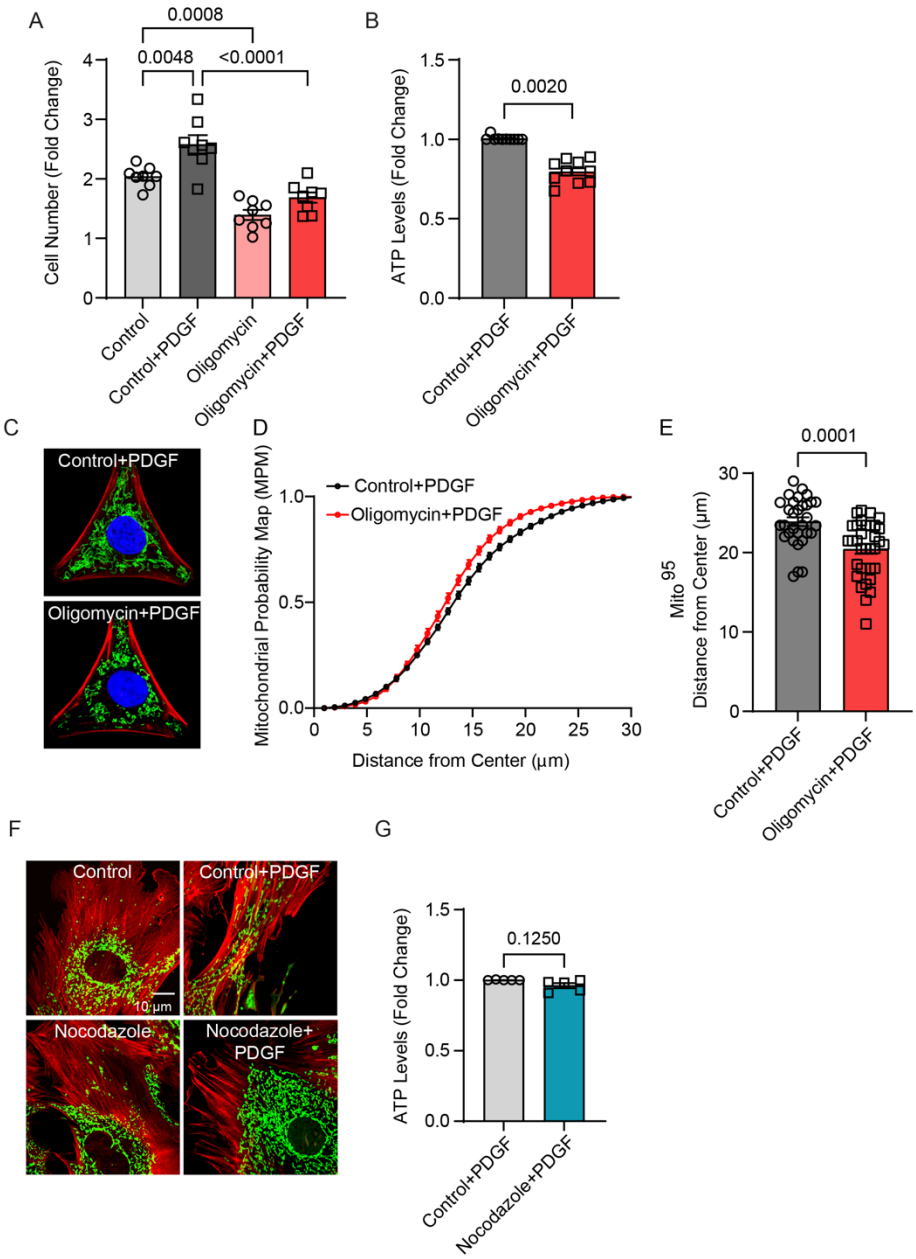


**Figure 4. Inhibition of mitochondrial ATP production reduces VSMC proliferation, but inhibiting mitochondrial mobility does not affect ATP levels.**

(**A**) Number of WT VSMCs after 72-hr treatment with either PDGF (20 ng/ml) and/or oligomycin (1 µM).
(**B**) ATP levels in WT VSMCs after 16-hr treatment with PDGF (20 ng/ml) or with PDGF in addition to oligomycin (1 µM).
(**C**) Representative confocal images of WT VSMCs on CYTOOchips™ with Y-shaped micropatterns, following 16-hr treatment with PDGF (20 ng/ml) and oligomycin (1 µM). Mitochondria, green; phalloidin, red; DAPI, blue.
(**D**) Mitochondrial probability map. The cumulative distribution of mitochondria was assessed for images as in (C) by modified Sholl's analysis.

(**E**) $Mito^{95}$ values, defined as the distance from the center of the Y-shaped pattern at which 95% of the mitochondrial signal is found for growing cells like in (C).
(**F**) Representative confocal images of WT VSMCs infected with mitoGFP and stained with phalloidin. Cells were synchronized by serum starvation for 48 hr and then released from starvation by replacing the medium with one containing 10% FBS and PDGF (20 ng/ml). Some samples were treated with nocodazole (1 µM). Images were taken immediately after growth media (Control) or growth media with nocodazole was added (Nocodazole) and after incubation for 16 hr (Control + PDGF, Nocodazole + PDGF).
(**G**) ATP levels in WT VSMCs after 16-hr treatment in growth media with PDGF or growth media supplemented with PDGF and Nocodazole (1 µM).
Statistical analyses were performed by one-way ANOVA (A) or Mann-Whitney test (B, E, G).

Figure 5

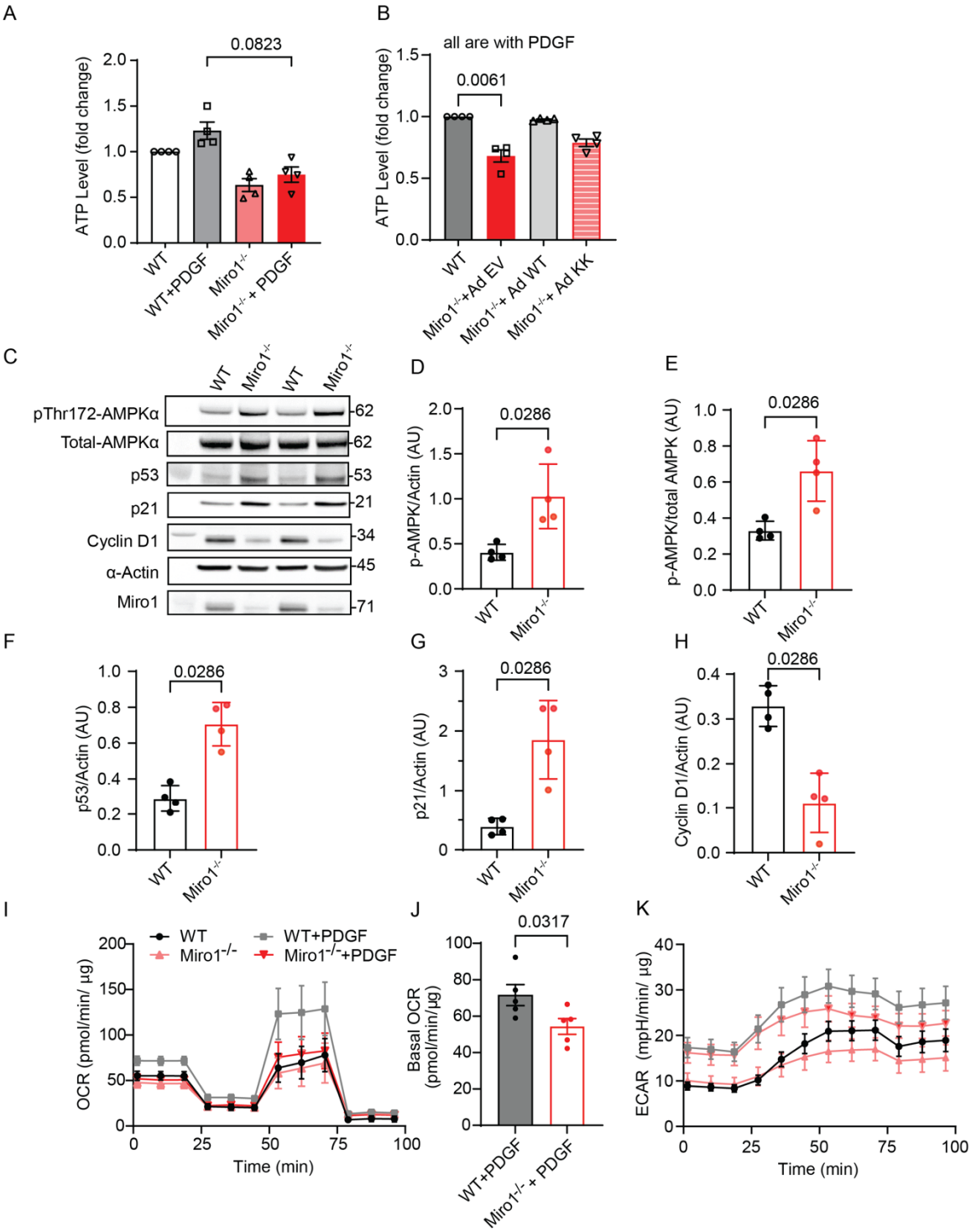


**Figure 5. Loss of Miro1 impairs mitochondrial metabolic activity and is associated with decreased proliferative capacity.**

(**A**) Intracellular ATP levels in WT and Miro1$^{-/-}$ VSMCs after treatment with PDGF (20 ng/ml for 16 hr) or control (no PDGF), normalized to levels in control WT VSMCs (no PDGF).

(**B**) Intracellular ATP levels in WT and Miro1$^{-/-}$ VSMCs transduced with adenovirus expressing MIRO1-WT (Ad WT) or MIRO1-KK (Ad KK) or control adenovirus (empty vector, Ad-EV) after treatment with PDGF (20 ng/ml for 16 hr) or control (no PDGF), normalized to ATP levels in control WT VSMCs (no PDGF).
(**C**) Immunoblot of lysates from WT and Miro1$^{-/-}$ VSMCs for markers of the metabolic state (phosphorylated (p-Thr172) and total AMPK$\alpha$), and cell cycle progression (p53, p21 and cyclin D1) at 48 hr after incubation in serum-free medium (cell-cycle arrest).
(**D-H**). Quantification of immunoblot signal in samples shown in (C) for (D) phosphorylated (p-Thr172) AMPK$\alpha$ normalized to actin, (E) phosphorylated (p-Thr172) AMPK$\alpha$ normalized to AMPK$\alpha$, (F) p53, (G) p21, and (H) cyclin D1, all normalized to actin.
(**I**) Oxygen consumption rate (OCR), as determined by Seahorse, for WT and Miro1$^{-/-}$ VSMCs with and without PDGF treatment (20 ng/ml for 16 hr).
(**J**) Quantification of basal OCR for WT and Miro1$^{-/-}$ VSMCs treated with PDGF (n=5).
(**K**) Extracellular acidification rate (ECAR), as determined by Seahorse, for WT and Miro1$^{-/-}$ VSMCs with and without PDGF treatment (20 ng/ml for 16 hr).
Statistical analyses were performed by Friedman test (A, B), and Mann-Whitney (D-H, J).

Figure 6

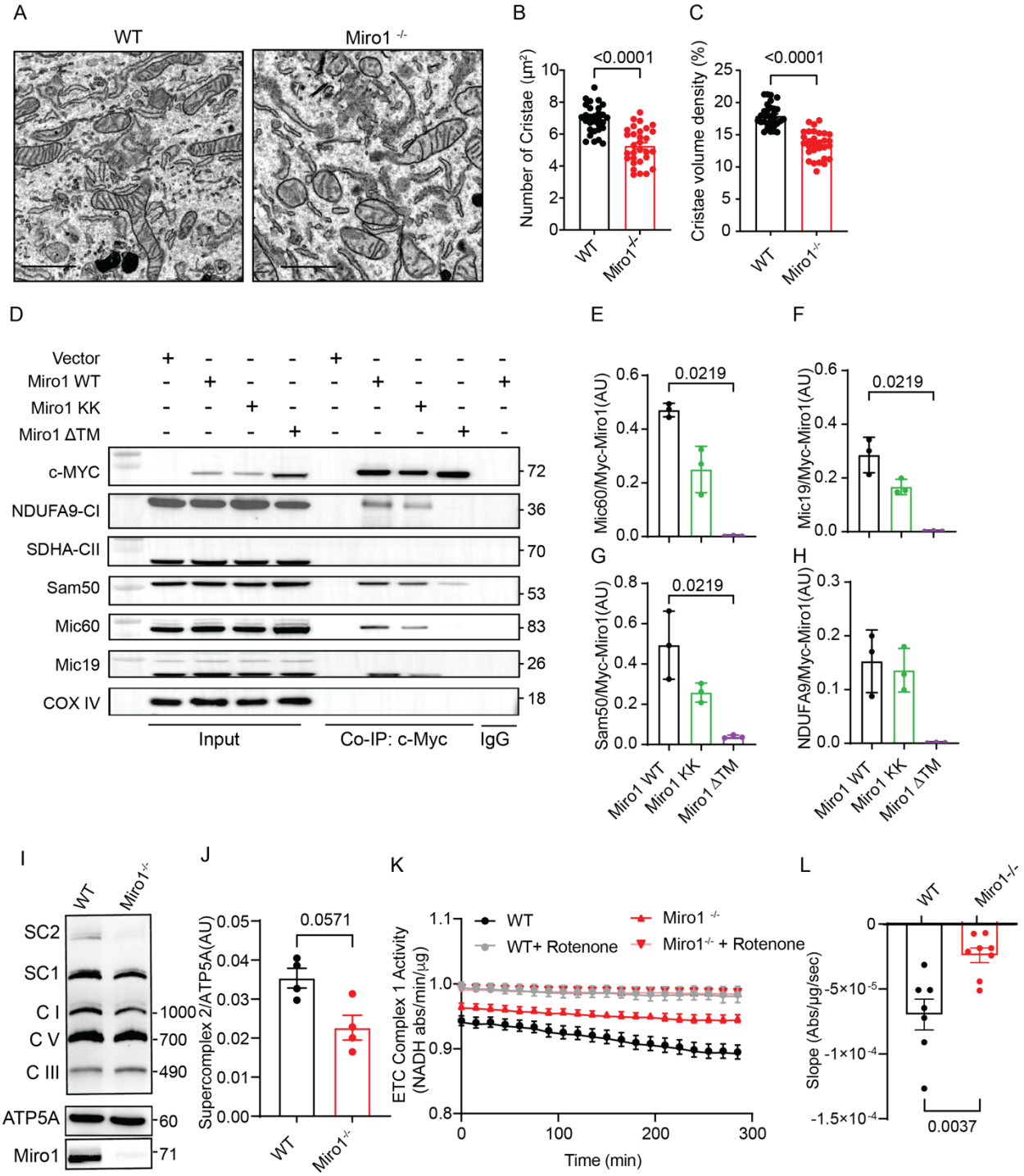


**Figure 6. Loss of Miro1 leads to dysregulation of ETC activity under growth conditions.**

(**A**) Transmission electron microscopy images of WT and Miro1$^{-/-}$ VSMCs.
(**B, C**) Quantification of (B) the number of mitochondrial cristae and (C) the volume density of the mitochondrial cristae in WT and Miro1$^{-/-}$ VSMCs.

(**D**) Levels of c-myc tagged MIRO1-WT, c-myc tagged MIRO1-KK, or MIRO1-ΔTM and proteins of the MIB/MICOS complex in HEK cells following pull-down assay, as determined by immunoblotting. C-myc tagged Miro1 constructs were expressed in HEK cells for 72 hr before cell lysis and pull-down were performed.
(**E-H**) Quantification of (E) MIC60, (F) MIC19, (G) SAM 50, and (H) NDUFA9 from (D), adjusted for immunoprecipitated c-myc-tagged MIRO1 as in (C).
(**I**) Levels of mitochondrial supercomplex and ETC subunits in WT and Miro1$^{-/-}$ VSMCs, as determined by blue-native poly-acrylamide gel electrophoresis (BN-PAGE).
(**J**) Quantification of supercomplex 2 in (I).
(**K**) Quantification of activity of ETC complex 1 in WT and Miro1$^{-/-}$ VSMCs, as determined by the decrease in the rate of absorbance at 340 nm with and without rotenone incubation for 10 min.
(**L**) Quantification of activity of ETC complex 1, plotted as the difference between absorbance curve slopes with and without rotenone (as in K).
Statistical analyses were performed by unpaired t-test (B, C), Kruskal-Wallis (E-H), Mann-Whitney (J, L).

Figure 7

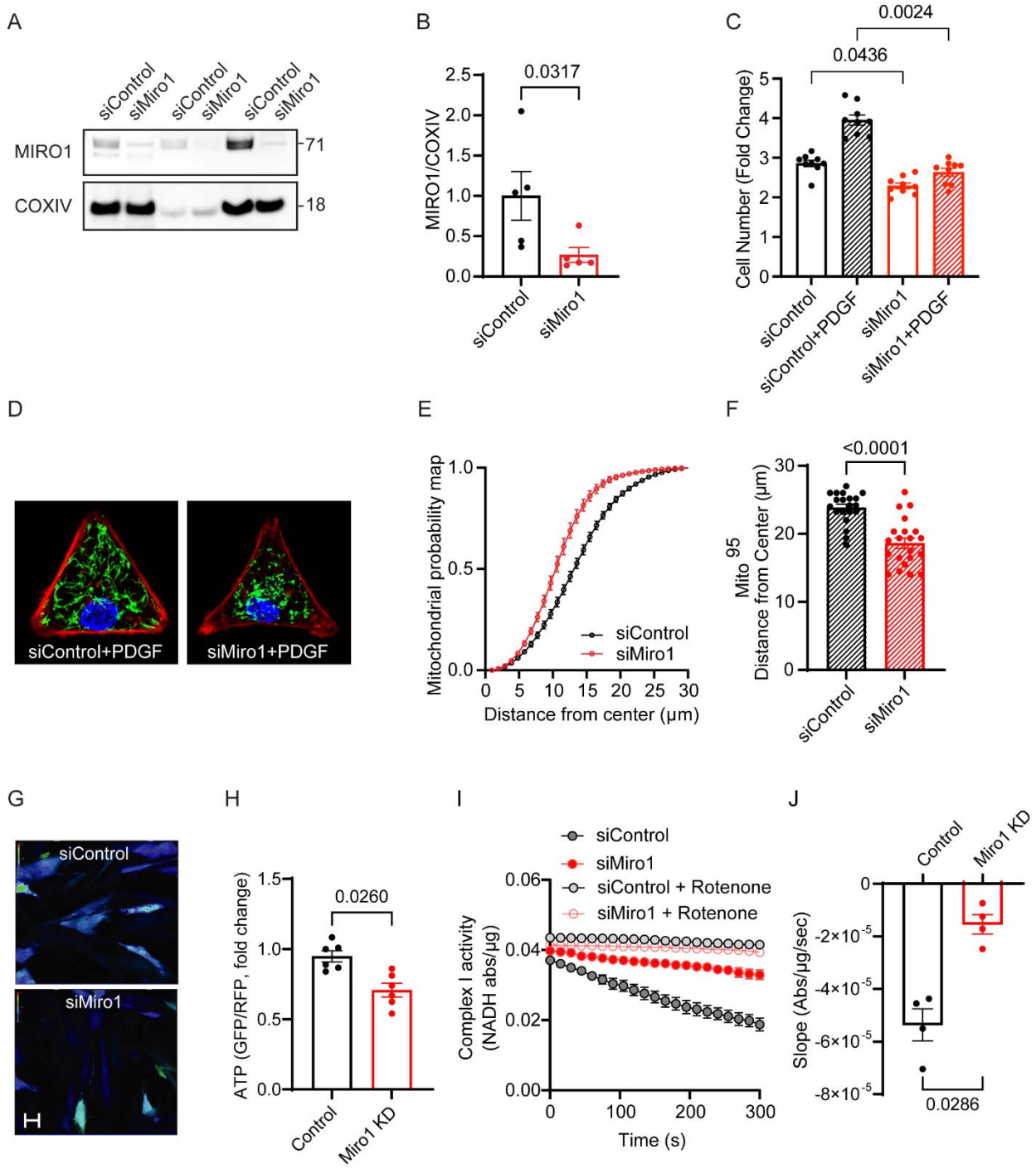


**Figure 7. MIRO1 knockdown in human coronary artery smooth muscle cells inhibits mitochondrial mobility, mitochondrial metabolism and proliferation.**
(**A**) Immunoblot for MIRO1 and COV IV in mitochondrial fractions of lysates from human coronary artery smooth muscle cells transfected with siControl or siMiro1 for 72 hr.
(**B**) Quantification of immunoblot signal in samples as shown in (A).

(**C**) Number of human coronary artery smooth muscle cells transfected with siControl or siMiro1 at 72 hr after incubation with growth media in addition to PDGF (20 ng/ml) or control.
(**D)** Confocal images of human coronary artery smooth muscle cells grown on CYTOOchips$^{TM}$. Cells were transfected with siControl or siMiro1 for 72 hr before being seeded onto CYTOOchips$^{TM}$. The cell cycle was synchronized by serum starvation for 24 hr (not shown); the cells were subsequently treated with medium containing 10% FCS and PDGF (20 ng/ml) for 6 hr.
(**E**) Mitochondrial probability map. The cumulative distribution of mitochondria was assessed for images as in (D) by modified Sholl's analysis.
(**F**) Mito$^{95}$ values, defined as the distance from the center of the CYTOOchips$^{TM}$ at which 95% of the mitochondrial signal is found, under the conditions used in (D).
(**G**) Images of human coronary artery smooth muscle cells transfected with siControl or siMiro1 at 72 hr after transduction with an adenovirus expressing a cytoplasmic ATP sensor with red reference protein (cyto-Ruby3-iATPSnFR1.0) for 24 hr.
(**H**) Quantification of GFP/RFP ratios, indicating cytosolic ATP levels in cells shown as in (G).
(**I**) Quantification of activity of ETC complex 1 in human coronary artery smooth muscle cells following transfection with siControl or siMiro1 as determined by the decrease in the rate of absorbance at 340 nm with and without rotenone incubation for 10 min.
(**J**) Quantification of activity of ETC complex 1, plotted as the difference between absorbance curve slopes with and without rotenone (as in I).
Statistical analyses were performed by Mann-Whitney (B, F, H, J) and Kruskal-Wallis (C).